ELSEVIER

Chemical Engineering Journal 117 (2006) 187–195

Chemical Engineering Journal

www.elsevier.com/locate/cej

Multi-scale flow behavior in gas–solids two-phase flow systems

B. Wu, L. Briens *, J.-X. Zhu

Department of Chemical and Biochemical Engineering, The University of Western Ontario, London, Ont., Canada N6A 5B9

Received 11 May 2005; received in revised form 9 November 2005; accepted 23 November 2005

Abstract

Differential pressure along the axis and local solids concentration in the fully developed region were measured in a high-density downer (0.025 m i.d., 5 m high). Chaos analysis was used to study the non-linear and multi-scale flow behavior in the downer. Local solids concentration measurements and global differential pressure measurements in the fully developed region were used to estimate the correlation integral. Pressure fluctuations in the fully developed region of the downer showed bi-fractal behavior. Large-scale behavior corresponded to a low correlation dimension, and small-scale behavior corresponded to a high correlation dimension. FCC particles showed more significant bi-fractal behavior than glass beads. Local flow dynamics from solids concentration measurements were contributed by solids flow of many different scales, namely dispersed particles and clusters of different sizes, so that there was only one scaling region in the log–log plot of correlation integral versus distance. Solids flux was found to significantly affect the correlation dimension.

Keywords: Downer; Chaos analysis; Flow dynamics; High flux; Solids concentration; Pressure fluctuation; Multi-scale

1. Introduction

In gas–solid two-phase systems, there are many flow behaviors at different scales due to the strong interactive effects between the particles and the gas. For example, gas-phase turbulence, particulate turbulence and cluster behavior all exist in the circulating fluidized bed (CFB). Generally, small-scale behavior corresponds to fluctuations of low amplitude and high frequency while large-scale behavior corresponds to fluctuations of high amplitude and low frequency [1]. Fluctuations are important as they promote distribution of the solids and the gas and without good distribution of the solids and gas there can be significant yield deviations across the downer. Therefore, characterization of the flow behavior according to scale is very important in understanding the flow dynamics and operation of gas–solid two-phase systems.

Fluidized beds have been recognized as chaotic systems since the early 1990s [2–4]. Since then, chaos analysis has been extensively used to characterize the flow behavior in fluidized bed systems. The correlation dimension is one of the most frequently calculated chaos parameters. It indicates the spatial complexity of the attractor in phase space and the number of dynamical degrees of freedom of the system [5]. A method proposed by Grassberger and Procaccia [6] has been frequently used to estimate the correlation dimension, and will be illustrated later in this paper.

Some researchers have reported two scaling regions in the logarithmic plot of correlation integral versus distance (r) and thus two correlation dimensions or bi-fractal behavior [1,7–13]. In these cases, the correlation dimension estimated from the scaling region at large distances was generally related to large-scale flow behavior and the correlation dimension estimated from the scaling region at small distances was related to small-scale flow behavior. Bai et al. [1] correlated the higher correlation dimension of small-scale behavior to particle motion, and the lower correlation dimension of large-scale behavior to the motion of voids; when the flow was dominated by dispersed particles in the fast fluidization regime, only one scaling region was observed and thus only one correlation dimension was estimated. Karamavruc and Clark [9] correlated the large-scale correlation dimension to slugs and the small scale to dispersed particles in the study of heat transfer in a slugging bed. Therefore, flow behavior of different scales in the gas–solid two-phase systems caused bi-fractal behavior. The appearance of two scaling regions in the log–log plot has also been discussed in other papers [14–18]. However, this bi-fractal phenomenon is not always reported in the study of fluidized bed systems characterized by the correlation dimension. This paper aims to further investigate

* Corresponding author. Tel.: +1 519 661 2111x88849; fax: +1 519 661 3498.
E-mail address: lbriens@uwo.ca (L. Briens).

1385-8947/$ – see front matter © 2005 Elsevier B.V. All rights reserved.
doi:10.1016/j.cej.2005.11.010

Nomenclature

CFB	circulating fluidized bed
$C_m(r)$	correlation integral at distance r for embedding dimension of m
D	correlation dimension
FCC	fluid catalytic cracking
G_s	solid flux (kg/m^2/s)
h	distance from the top entrance of the downer (m)
i.d.	inner diameter (m)
m	embedding dimension
o.d.	outer diameter (m)
r	distance between a pair of points on the attractor
U_g	superficial gas velocity (m/s)
V_p	particle velocity (m/s)
$\bar{\varepsilon}_s$	cross-sectional average solids holdup
ν	scaling factor
ρ_p	particle density (kg/m^3)
τ	time delay (units of time)

the multi-scale flow behavior in gas–solid systems using different measurements.

2. Experimental and operating procedures

Experiments were conducted in a high-density downer. A schematic diagram of the experimental apparatus is illustrated in Fig. 1. This cold-model gas–solids downflow fluidized bed was a 5 m tall plexiglass column of 0.025 m i.d. There were two conduits: one was the downer column and the other was the particle recycle line. One solids storage tank was on the top and the other one was at the bottom. Twelve pressure taps were installed along the downer column, located at 0.10, 0.30, 0.50, 0.70, 1.00, 1.20, 1.50, 1.70, 2.50, 2.70, 3.40 and 3.60 m from the top entrance of the column. Six differential pressure transducers were connected to the 12 taps to measure a distance of 0.2 m along the axial direction. Local solids concentration fluctuations were measured by a fibre optical solids concentration probe installed 2.6 m from the top entrance of the column, between the two taps located at 2.50 and 2.70 m at $r/R = 0.5$. Two pinch valves were installed 3.00 and 4.40 m from the top entrance to obtain the actual cross-sectional average solids holdup in the fully developed region by collecting the solids and measuring the height of the solids trapped between the two valves when they were closed simultaneously near the end of each experiment. The solids flux (G_s) was determined by a load cell installed underneath the bottom storage tank, which monitored the rate of mass change in the tank.

The solids feeder system included a particle feeder under the top storage tank, a vibrating pipe and a feeding funnel. The particle feeder was 0.20 m i.d. and 0.74 m tall. The upper part of the particle feeder was a packed bed, which ensured a constant static pressure to the solids. A movable tray was installed underneath a hole where the solids exit at the bottom of the upper part to act as a control valve of the solids flowrate. By changing the level and angle of the small movable tray, the particle feeder delivered a regulated amount of solids into the vibrating pipe. The vibrating pipe was 0.10 m i.d. and 1.35 m long. The pipe was at an angle of 20°, which was smaller than the angle of repose of the particles and further regulated the solids flowrate. A vibrator was installed on the outside of the pipe and located at the middle of the inclined pipe. Through vibration, particles flowed smoothly to the feeding funnel. The feeding funnel was 0.15 m tall, 0.25 m i.d. at the top part, and 0.025 m i.d. at the bottom part. The total height of the feeding funnel was 0.66 m. Solids were pre-accelerated by gravity in the feeding funnel before entering the downer column. Particles had an initial velocity close to the terminal velocity at the entrance of the downer [19] and therefore choking was avoided and high solids fluxes could be achieved.

Table 1
Operating conditions

Glass beads		FCC	
G_s (kg/m^2/s)	U_g (m/s)	G_s (kg/m^2/s)	U_g (m/s)
120	0.2	50	0.5
200	0.5	100	1.0
300	1.0	150	2.0
400	2.0	200	4.0
600	4.0	280	6.0
800	6.0	350	8.0
1000	8.0		

All experiments were conducted on a batch basis over a wide range of operating conditions listed in Table 1. The main gas flow was introduced at the top of the feeding funnel. The flowrate of the main gas was monitored by a rotameter and was the same as the gas flowrate in the downer column. Solids in the top tank flowed down through the particle feeder, passed through the inclined pipe, entered the feeding funnel together with gas, and flowed through the downer column to the bottom tank. Once solids and gas had fallen into the bottom storage tank, the solids were separated from the gas by gravity and deposited in the tank, and the gas flowed up through the exhaust gas pipe to a bag filter, where any remaining fine particles were collected before the gas entered the exhaust system. After each test, particles in the bottom tank were then entrained up through the recycle line (0.032 m i.d.) to the top tank. Entrained solids were separated from the gas by falling in the upper tank and then by two cyclones before entering the bag filter. The primary cyclone was 0.39 m tall and 0.10 m i.d. and the secondary cyclone was 0.26 m tall and 0.067 m i.d.

Glass beads of 2433 kg/m^3 (Geldart-B powders) and FCC particles of 1420 kg/m^3 (Geldart-A powders) were used for the tests. The mean particle diameters were 374.3 and 59 μm, respectively. All signals were sampled simultaneously at 1000 Hz with a time length of 60 s for each measurement. The A/D board (Lab-PC-1200, National Instruments) had 8 channels with 12 bit (1/4096) resolution. Low pass filter with a critical frequency of 65 Hz for the differential pressure signals and 250 Hz for the optical probe signals was applied before estimating the correlation dimension.

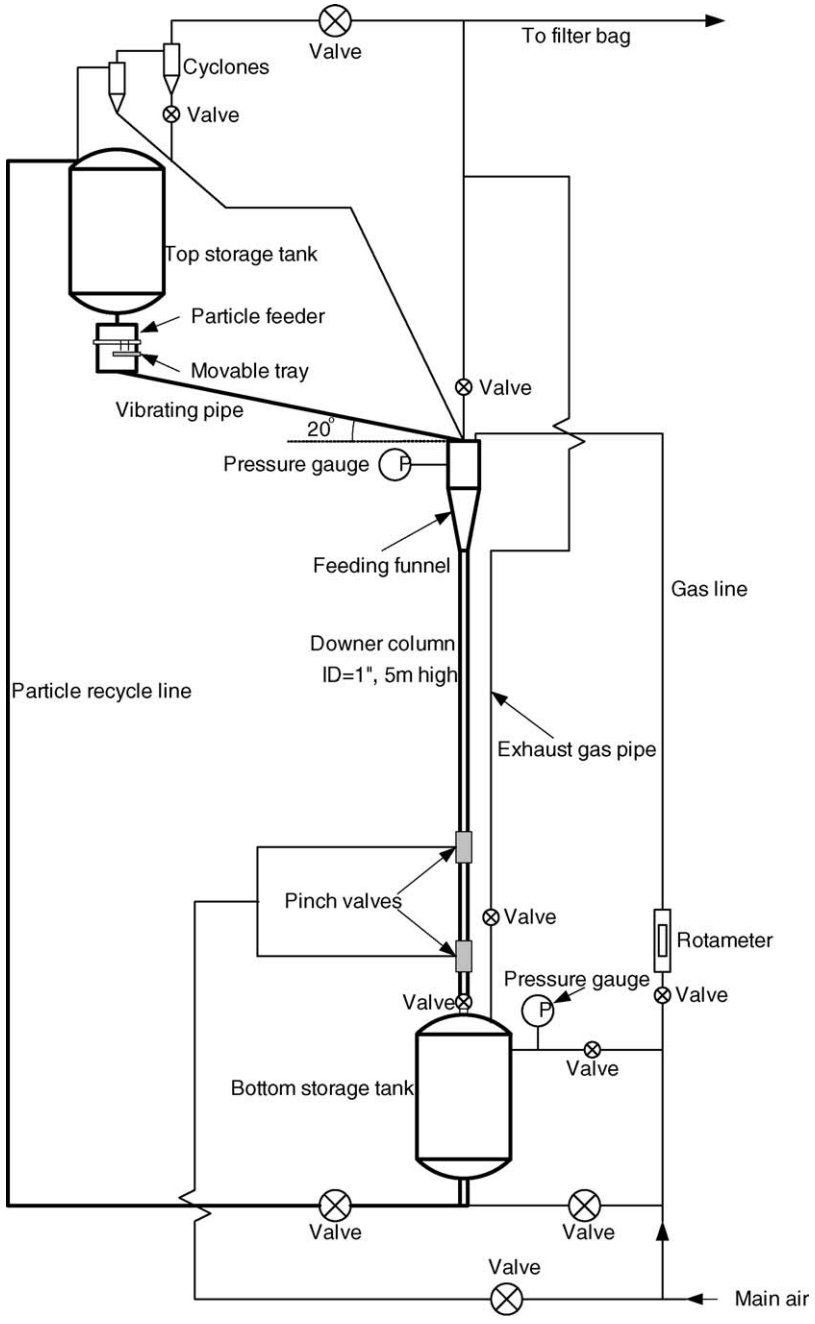

Fig. 1. Schematic diagram of the high-density downer.

The solids concentration probe had a very tiny tip and only measured the solids concentration very close to the tip. The flow dynamics captured by the probe were thus very local volumetrically. The tip of the probe was always located at a dimensionless radial position of $r/R = 0.5$. The differential pressure fluctuations reflected the pressure fluctuations mainly between the two measurement ports along the axis of the downer with a distance of 0.2 m. The measured pressure fluctuations, however, also had contributions from the flow behavior above the upper measurement port and below the bottom measurement port. Therefore, flow dynamics captured by pressure fluctuations were more global volumetrically.

3. Estimation of correlation dimension

The correlation dimension was estimated using the method proposed by Grassberger and Procaccia [6]. The correlation integral, C_m, is calculated at various distances, r, and embedding dimensions, m:

$$C_m(r, m) = \frac{2}{N_m(N_m - 1)} \sum_{i=1, j=i+1}^{N_m} \theta(r - r_{ij}) \quad (1)$$

The scaling factor, ν, is then calculated from the slope of the linear region of the plot of $\ln C_m(r, m)$ versus $\ln(r)$. If ν does

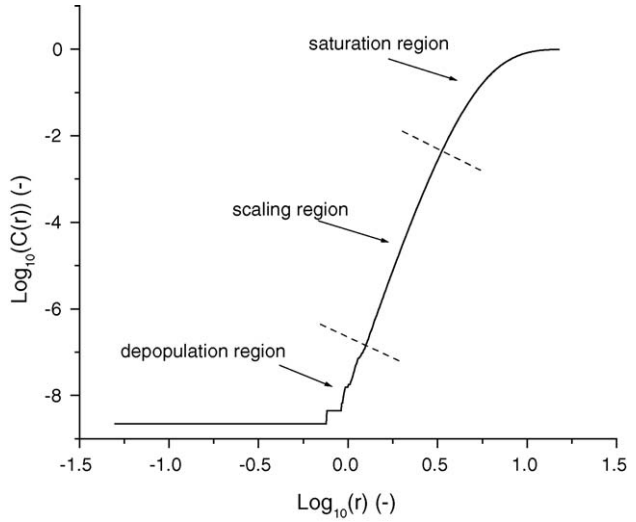

Fig. 2. An example of log–log plot of correlation integral vs. r.

not change with an increase in m, the scaling factor ν is equal to the correlation dimension (D). Embedding dimension, m, was at least 18 in this study according to Takens [20].

A typical example of a log–log plot of correlation integral versus distance r is shown in Fig. 2. There are generally three regions: for r close to or greater than the diameter of the attractor, the correlation integral does not increase with increasing r, and this region is called the saturation region; when r is smaller than the smallest distance between phase space pairs, the correlation integral should be zero and the region is called the depopulation region; an intermediate linear part is the scaling region for calculating the scaling factor ν [21]. An example of a plot that has two scaling regions, or that shows bi-fractal behavior, is shown in Fig. 3. The two scaling regions are separated by a transition region. The curve was fitted and the scaling factors ν_1 and ν_2 were then estimated from the two local maxima of the first derivative of the fitted curve.

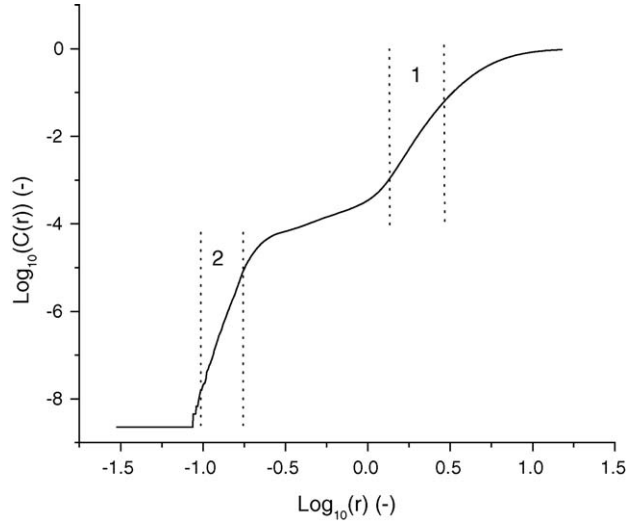

Fig. 3. An example of bi-fractal behavior.

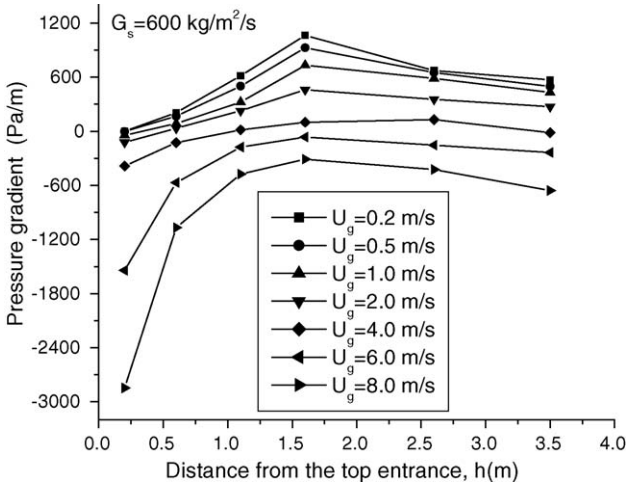

Fig. 4. Axial profiles of pressure gradient using glass beads.

4. Results and discussion

4.1. Axial flow development from pressure gradient

An example of time-averaged pressure gradient profiles along the axial direction of the downer column is shown in Fig. 4. Pressure gradients increased rapidly along the downer column within the initial 1–2 m, and then became approximately constant. The slight drop of pressure gradient past 1.5 m at lower U_g ($\leq$1.0 m/s) may be caused by solids deceleration due to the high velocity particle feeding and low velocity operation. The constant pressure gradients indicated that the particles had reached a constant velocity. Axial profiles of pressure gradients under other operating conditions showed similar trends for both the glass beads and FCC particles with the acceleration length for the FCC particles slightly shorter than that for the glass beads. Therefore, the acceleration region was estimated to be within approximately 1–2 m from the top entrance of the downer.

4.2. Distinguishing between local and global measurements

Segments of time series from local solids concentration measurements and differential pressure measurements are shown in Fig. 5. Small and large fluctuations were distributed throughout the solids concentration signals, while the pressure signals were dominated by large and slow fluctuations. Solids concentration measurements from the optical probe indicate a local flow behavior. The small and rapid fluctuations were possibly due to dispersed particles while the larger fluctuations were more likely due to clusters. Pressure measurements indicated global volumetric flow behavior, and thus there were large fluctuations in the signals. As the pressure measurements were also affected by the flow of dispersed particles and clusters, there were also some smaller fluctuations in the signals. Local and global flow dynamics were thus observed to be different directly from the time series.

Correlation integrals were estimated from time series of solids concentration measurements and differential pressure measurements. All the correlation integrals shown in this study

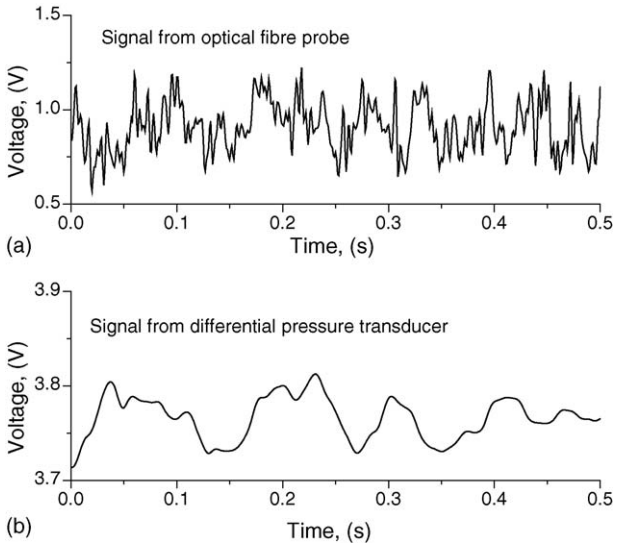

Fig. 5. Time series of signals measured simultaneously by the pressure transducer and fibre optical probe in the downer section of 2.5–2.7 m using glass beads at $G_s = 400\,kg/m^2/s$ and $U_g = 0.2\,m/s$. (a) Signal from optical fibre probe and (b) signal from differential pressure transducer.

were estimated using an embedding dimension of at least 18, which was verified to be sufficiently large to correctly reconstruct the attractor. For solids concentration measurements, only one scaling region was found in the logarithmic plots of correlation integral versus r, similar to the plot shown in Fig. 2. As shown in Fig. 6, for most pressure measurements, two scaling regions were identified from the logarithmic plots of correlation integral versus r. For pressure measurements in the top entrance region ($h < 1.0\,m$) under low superficial gas velocities ($U_g \leq 2\,m/s$) using glass beads particles, only one scaling region was observed. Therefore, in the fully developed region, pressure measurements could be easily distinguished from solids concentration measurements by the correlation integral, as only the pressure measurements showed bi-fractal behavior.

In order to directly examine the flow dynamics, attractors were reconstructed from time series of pressure and concentration measurements and shown in two dimensions in Figs. 7 and 8. The attractor for the concentration measurements had a more complex shape than the attractor reconstructed from pressure measurements. The trajectories of the attractor of pressure measurements were smoother than those of the concentration measurement attractor. However, considering the attractors drawn as scattered points, it appeared that there were some relatively dense regions, mostly close to the core, of the attractor of pressure measurements, while there were no obviously dense regions of the attractor of concentration measurements. The relatively dense region may have caused the scaling region at small distances r and thus the observed bi-fractal behavior for the pressure measurements.

4.3. Multi-scale flow behavior in the high-density downer

Fig. 9 shows time series of pressure measurements at different axial levels. Pressure fluctuations were not significant in

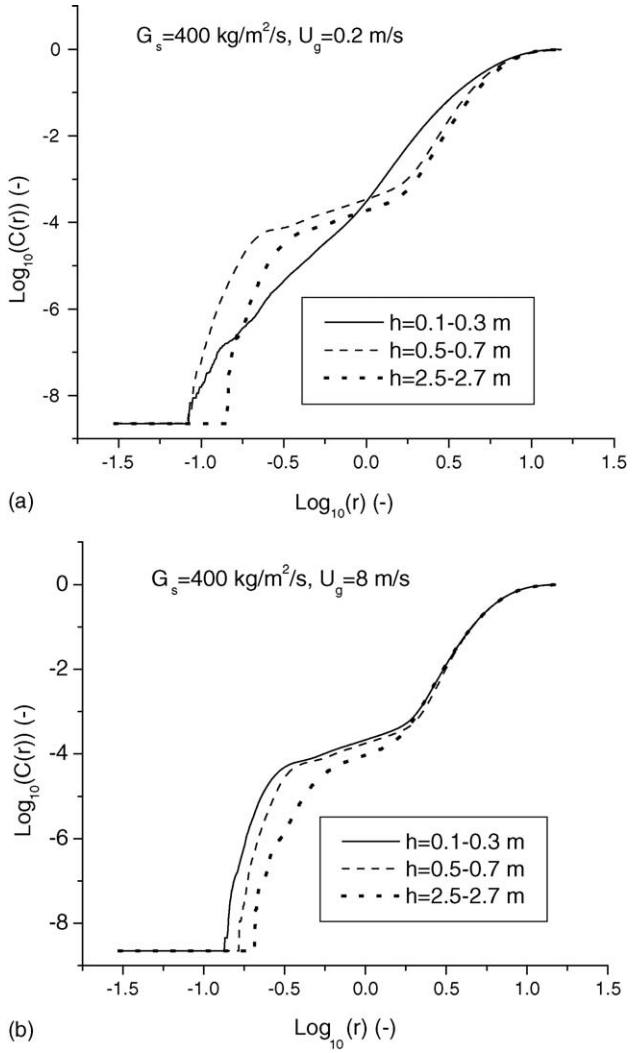

Fig. 6. Correlation integral vs. r at different axial levels for pressure measurements using glass beads. (a) $G_s = 400\,kg/m^2/s$ and $U_g = 0.2\,m/s$ and (b) $G_s = 400\,kg/m^2/s$ and $U_g = 8\,m/s$.

the top entrance region due to very low solids velocities. Dispersed particles and aggregates of different sizes existed in the top entrance region of the downer. They contributed to the pressure fluctuations although their contribution was relatively weak. Therefore, only one scaling region was found (Fig. 6a). Further along the downer axis (0.5–0.7 m), the solids velocity was higher due to acceleration. Large clusters with high momentum contributed more significantly to the pressure fluctuations and caused strong cyclic behavior. Therefore, two scaling regions appeared (Fig. 6). At a high U_g of 8 m/s, two scaling regions were found from pressure measurements at all axial levels of the downer.

Results found in this study are comparable to those from Zhao et al. [11] in a bubbling bed using pressure measurements. When the fluidized bed was in the particulate regime, only one scaling region was identified; in the bubbling regime, two scaling regions appeared. The correlation dimension of large-scale behavior was attributed to the bubbles and the correlation dimension of small-scale behavior was attributed to the dense phase.

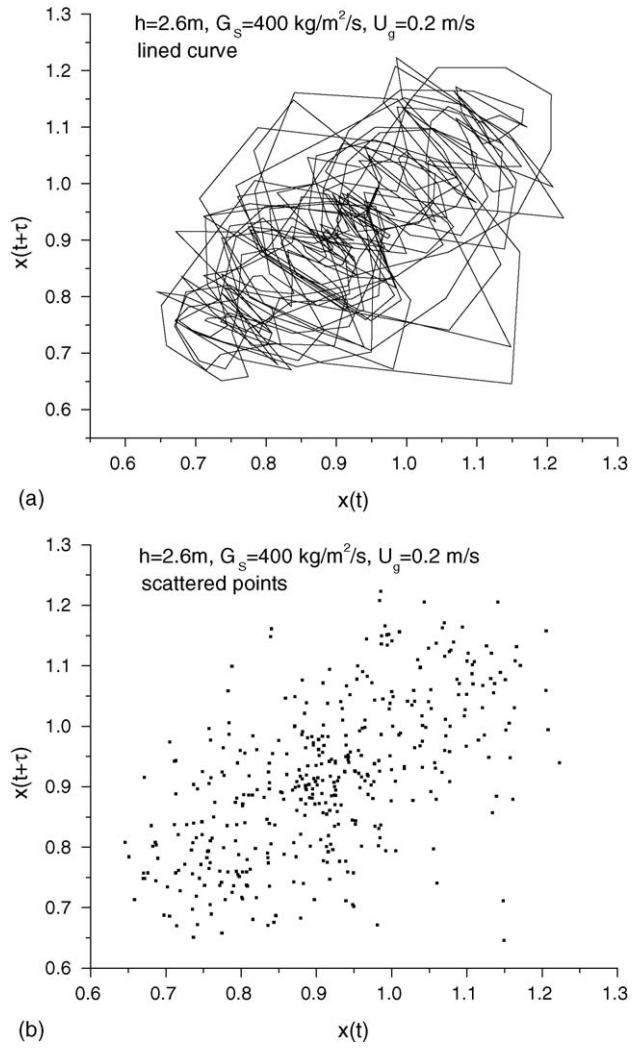

Fig. 7. Attractor reconstruction from time series of solid concentration measurements in fully developed downer using glass beads. (a) $h = 2.6$ m, $G_s = 400$ kg/m^2/s, $U_g = 0.2$ m/s, lined curve and (b) $h = 2.6$ m, $G_s = 400$ kg/m^2/s, $U_g = 0.2$ m/s, scattered points.

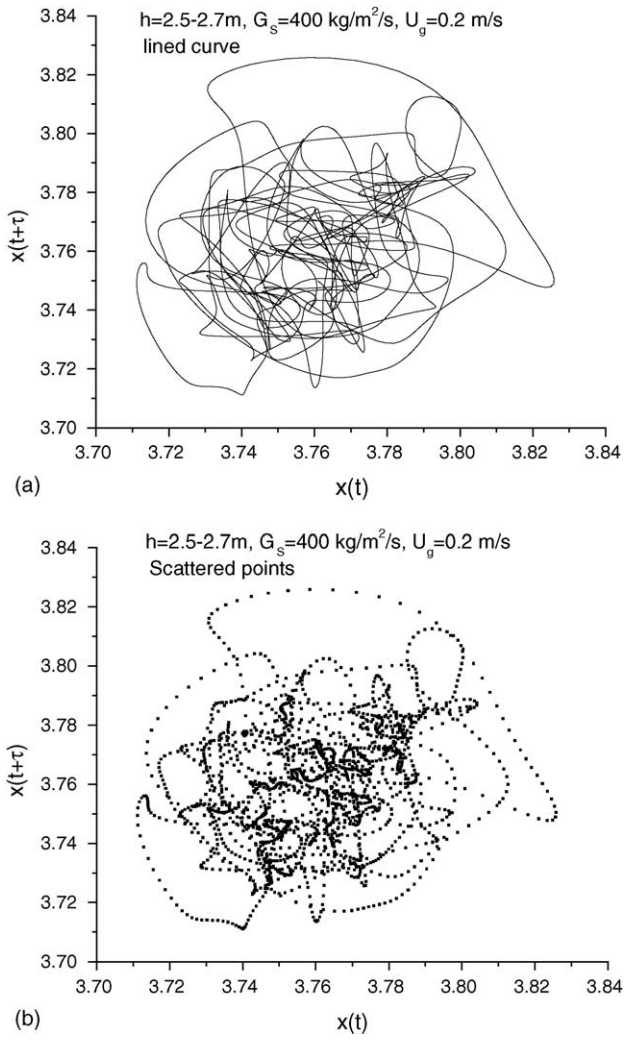

Fig. 8. Attractor reconstruction from time series of pressure measurements in fully developed downer using glass beads: (a) $h = 2.5$–2.7 m, $G_s = 400$ kg/m^2/s, $U_g = 0.2$ m/s, lined curve and (b) $h = 2.5$–2.7 m, $G_s = 400$ kg/m^2/s, $U_g = 0.2$ m/s, scattered points.

Therefore, dense flow in the top entrance region of the downer was likely in particulate regime with the dominant effect of clustering behavior on pressure fluctuations in the fully developed region of the downer similar to the dominant effect of bubble/gas behavior on the pressure fluctuations in conventional fluidized beds.

A comparison of the correlation integrals estimated from pressure measurements and solids concentration measurements in the fully developed region is shown in Fig. 10. The correlation dimensions of small-scale and large-scale behavior from pressure measurements were 11.6 and 5.8, respectively. The correlation dimension estimated from solids concentration measurements was 10.6. Local flow behavior ($D = 10.6$) was more complex than the global flow ($D_1 = 5.8$) but more regular than the small-scale flow behavior ($D_2 = 11.6$) of the pressure fluctuations, since large-scale flow behavior of clusters also contributed to local solids concentration fluctuations.

Fig. 11 shows a comparison of the correlation integrals estimated from the pressure measurements for FCC particles and

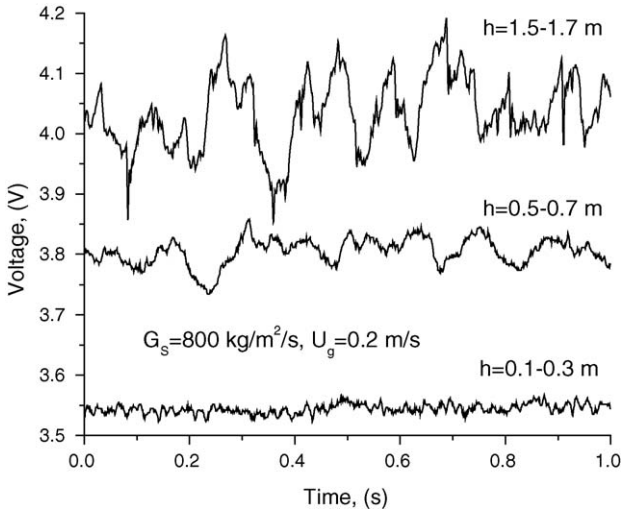

Fig. 9. Time series of pressure measurements in the downer using glass beads.

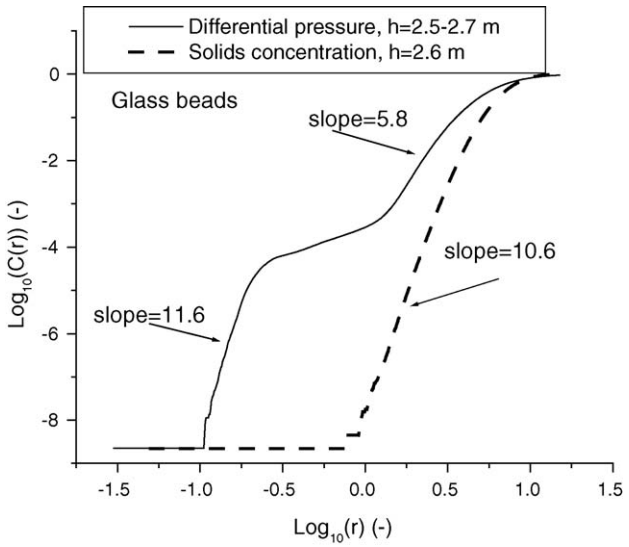

Fig. 10. Comparison of correlation integrals from different measurements at $G_s = 120\,kg/m^2/s$, $U_g = 0.2\,m/s$.

glass beads in the fully developed region. There are two scaling regions for both solids indicating multi-scale behavior. The scaling regions are separated by a transition region. The length of the transition region reflects the difference in the scales. The transition region was wider for the FCC particles than for the glass beads. According to the continuous equation of solids: $\rho_p \bar{\varepsilon}_s v_p = G_s$, where G_s is solids flux, v_p the particle velocity, ρ_p the particle density, and $\bar{\varepsilon}_s$ is the cross-sectional average solids holdup, the particle density and terminal velocity of glass beads were much higher than those of FCC particles. Therefore, the cross-sectional average solids holdup for glass beads was much lower than that of FCC particles at the same G_s and U_g. Therefore, FCC particles (Geldart-A) formed large clusters more readily compared to glass beads (Geldart-B). Large clusters of FCC particles caused much stronger cyclic behavior (Fig. 12). As the scale difference between the large clusters and dispersed particles/small clusters was significant, the transition region of

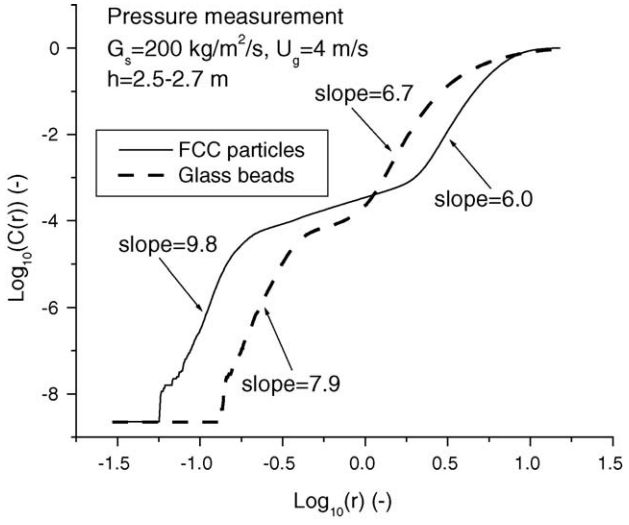

Fig. 11. Comparison of correlation integral for different particles.

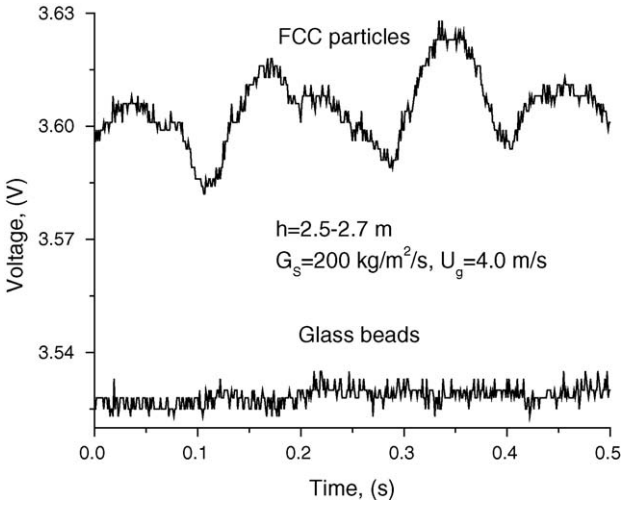

Fig. 12. Time series of pressure measurements using different particles.

the correlation integral was longer for FCC particles than for glass beads. Larger clusters of FCC particles caused a lower correlation dimension ($D = 6.0$) compared to that of glass beads ($D = 6.7$), as larger clusters caused more regular pressure fluctuations. Small-scale flow behavior of finer FCC particles caused a larger correlation dimension ($D = 9.8$) compared to that of glass beads ($D = 7.9$), as fine particles caused irregular and small pressure fluctuations.

Fig. 13 shows profiles of correlation dimension as a function of G_s for both pressure and solids concentration measurements at U_g of 0.2 m/s using glass beads. For solids concentration measurements, D decreased with increasing solids flux at low G_s (<400 kg/m^2/s). Under these conditions, the flow was dilute with intermittent passage of particles and small clusters. At high solids fluxes of 400–800 kg/m^2/s, D was lower and almost

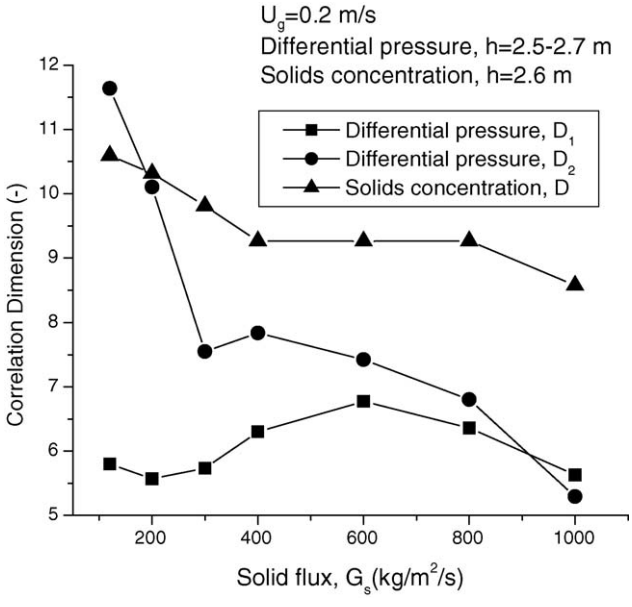

Fig. 13. Correlation dimensions estimated from differential pressure measurements and solids concentration measurements using glass beads as a function of G_s.

constant. Under these conditions, as G_s increased more clusters were formed. These clusters might lead to a dense flow condition that occupied the whole cross-section. Such local dense flow might be similar to the dense suspension upflow (DSU) [22] suggested in a high-density riser. However, the size of the clusters in the downer did not significantly increase due to high slip velocities between clusters and the gas flow. Large clusters caused regular flow while more clusters caused irregular flow. This competing change in fluctuation behavior resulted in almost constant D values over high solids fluxes from 400 to 800 kg/m^2/s. High-flux flow was therefore identified at over 400 kg/m^2/s. At a very high solids flux of 800 kg/m^2/s, D decreased slightly with increasing G_s as the fluctuations from the large clusters became significant. D was affected more significantly by large and slow fluctuations than small rapid fluctuations at very high solids flux.

Similar to D from local solids concentration measurements, D_2 estimated from small scales of differential pressure measurements decreased with increasing G_s under low-flux flow (<300 kg/m^2/s). Small-scale pressure fluctuations were dominant under low-flux flow and were very irregular resulting in a very high D_2. Small-scale behavior was damped with increasing G_s and D_2 decreased. Large-scale behavior under low-flux flow (<400 kg/m^2/s) was slow, weak and regular with very small D_1 due to small clusters. D_1 became higher under high-flux flow (400–800 kg/m^2/s), due to enhanced clustering behavior. More clusters caused irregular pressure fluctuations, while large clusters caused large and regular pressure fluctuations. This competing flow behavior of clusters also resulted in almost constant D_1 over high solids fluxes from 400 to 800 kg/m^2/s. Small-scale behavior was further damped with increasing G_s and D_2 kept decreasing. D_1 and D_2 became closer under high-flux flow due to regular behavior for both small and large scales under dense flow. At very high G_s (>800 kg/m^2/s), more and larger clusters caused more regular pressure fluctuations across many scales, so that D_1 and D_2 decreased and became very close.

D estimated from local solids concentration measurement was generally much higher than those from global differential pressure measurements (both D_1 and D_2), indicating extremely complex local flow dynamics and relatively regular global flow dynamics. This reflects the different flow properties of the downer system. Even though correlation dimensions from local and global flow behaviors showed different values under same operating conditions, some similar transitions with increasing G_s indicated that flow properties could be captured by both local and global flow dynamics.

Considering the small diameter of the downer (0.025 m i.d.), there may have been wall effects on the solids and gas distributions in the downer and thus on the fluid dynamics. This would affect the absolute value of the correlation dimension. However, the multi-scale flow behavior has been confirmed from preliminary pressure fluctuation measurements in a 0.20 m i.d. riser (10 m high) using FCC particles by authors. Therefore, multi-scale flow should be a characteristic of two-phase flow systems. For solids concentration measurements, only one scaling region of log–log plot of correlation integral versus r was found in the 0.20 m i.d. riser circulating fluidized beds at different axial and radial position. However, further measurements in denser beds (e.g., bubbling or turbulent bed) should be considered.

5. Conclusions

Local solids concentration measurements and global differential pressure measurements in the fully developed region of a high-density downer were distinguished by estimation of the correlation integral: the log–log plot of correlation integral versus r from solids concentration measurements had only one scaling region; two scaling regions were usually identified from pressure measurements.

Pressure fluctuations in the fully developed region of the downer were dominated by strong cyclic behavior from large clusters. The dominant cyclic behavior caused the large difference in temporal scales in the time series of pressure fluctuations, so that bi-fractal behavior was observed. Large-scale behavior corresponded to a low correlation dimension, and small-scale behavior corresponded to a high correlation dimension. FCC particles (Geldart-A) easily formed clusters compared to glass beads (Geldart-B), so that bi-fractal behavior was more significant from pressure measurements in the fully developed region compared to glass beads under the same operating conditions.

Local flow dynamics from solids concentration measurements were almost equally influenced by flow behavior at many different scales, namely dispersed particles and clusters of different sizes. Local flow behavior from solids concentration measurements in the developed region of the downer was generally more complex than the global flow behavior from pressure measurements.

Comparisons of small and large scales flow behavior from differential pressure measurements were drawn from D_1 and D_2. Even though correlation dimensions from local and global flow behavior showed different values under the same operating conditions, some similar transitions with increasing G_s indicated that flow properties could be captured by both local and global flow dynamics.

Acknowledgements

The authors are grateful to the Natural Sciences and Engineering Research Council of Canada for the financial support. Bangyou Wu would like to thank Dr. Q. Zhao and Joshua Smit for their help with the experiments.

References

[1] D. Bai, H. Bi, J.R. Grace, Chaotic behavior of fluidized beds based on pressure and voidage fluctuations, AIChE J. 43 (5) (1997) 1357–1361.
[2] J. Stringer, Is a fluidized bed a chaotic dynamic system? in: Proceedings of the10th International Conference on Fluidized Bed Combustion, vol. 1, 1989, pp. 265–272.
[3] C.S. Daw, J.S. Halow, Characterization of voidage and pressure signals from fluidized beds using deterministic chaos theory, in: E.J. Anthony (Ed.), Proceedings of the 11th International Conference on Fluidized Bed Combustion, vol. 2, ASME, 1991, pp. 777–786.
[4] C.M. van den Bleek, J.C. Schouten, Deterministic chaos: a new tool in fluidized bed design and operation Chem. Eng. J. 53 (1993) 75–87.

[5] M.L.M. van der Stappen, Chaotic hydrodynamics of fluidized beds, Ph.D. Thesis, Delft University of Technology, The Netherlands, Delft University Press, 1996.
[6] P. Grassberger, I. Procaccia, Characterization of strange attractors, Phys. Rev. Lett. 50 (5) (1983) 346–349.
[7] F. Franca, M. Acigoz, R.T.J. Lahey, A. Clausse, The use of fractal techniques for flow regime identification, Int. J. Multiphase Flow 17 (4) (1991) 545–552.
[8] B. Izrar, F. Lusseyran, Chaotic behavior of an annular film of liquid unstabilized by an interfacial shear stress, in: G. Gouesbet (Ed.), Instabilities in Multiphase Flows, Plenum, New York, 1993, pp. 1–15.
[9] A.I. Karamavruc, N.N. Clark, Local differential pressure analysis in a slugging bed using deterministic chaos theory, Chem. Eng. Sci. 52 (3) (1997) 357–370.
[10] D. Bai, A.S. Issangya, J.R. Grace, Characteristics of gas-fluidized beds in different flow regimes, Ind. Eng. Chem. Res. 38 (3) (1999) 803–811.
[11] G.B. Zhao, Y.F. Shi, G.Q. Guan, H.R. Yu, in: M. Kwauk, J. Li, W.C. Yang (Eds.), Chaotic Method for Distinguishing Between Particulate and Cluster Fluidization, Fluidization X, Engineering Foundation, New York, 2001, pp. 157–164.
[12] L. Huilin, D. Gidaspow, J.X. Bouillard, Chaotic behavior of local temperature fluctuations in a laboratory-scale circulating fluidized bed, Powder Technol. 123 (2002) 59–68.
[13] A. Ajbar, K. Alhumaizi, A. Ibrahim, M. Asif, Hydrodynamics of gas fluidized beds with mixture of group D and B particles, Can. J. Chem. Eng. 80 (2002) 281–288.
[14] A. Ben-Mizrachi, I. Procaccia, Characterization of experimental (noisy) strange attractors, Phys. Rev. A 29 (2) (1984) 975–977.
[15] J. Theiler, Spurious dimension from correlation algorithms applied to limited time-series data, Phys. Rev. A 34 (3) (1986) 2427–2432.
[16] J.X. Bouillard, A.L. Miller, Experimental investigations of chaotic hydrodynamic attractors in circulating fluidized beds, Powder Technol. 79 (3) (1994) 211–215.
[17] L. Huilin, D. Gidsapow, J.X. Bouillard, Dimension measurements of hydrodynamic attractors in circulating fluidized beds, Powder Technol. 90 (1997) 179–185.
[18] G.B. Zhao, J.Z. Chen, Y.R. Yang, Predictive model and deterministic mechanism in a bubbling fluidized bed, AIChE J. 47 (7) (2001) 1524–1532.
[19] W.D. Liu, K.B. Luo, J.-X. Zhu, J.M. Beeckmans, Characterization of high density gas–solids downflow fluidized beds, Powder Technol. 115 (2001) 27–35.
[20] F. Takens, in: D.A. Rand, L.-S. Young (Eds.), Detecting Strange Attractors in Turbulence, Lecture Notes in Mathematics, vol. 898, Springer Verlag, New York, 1981, pp. 366–381.
[21] L. Briens, Identification of flow regimes in multiphase reactors by time series analysis, Ph.D. Thesis, The University of Western Ontario, London, Canada, 2000.
[22] J.R. Grace, A.S. Issangya, D. Bai, H.-T. Bi, J.-X. Zhu, Situating the high-density circulating fluidized bed, AIChE J. 45 (10) (1999) 2108–2116.